Application of Low-Frequency Raman Spectroscopy to Probe Dynamics of Lipid Mesophase Transformations upon Hydration

Lasse S. Krog, Jacob J. K. Kirkensgaard, Vito Foderà, Ben J. Boyd,* and Kārlis Bērziņš*

Read Online

ACCESS | Metrics & More | Article Recommendations | Supporting Information

ABSTRACT: Low-frequency Raman (LFR) spectroscopy is presented as a viable tool for studying the hydration characteristics of lyotropic liquid crystal systems herein. Monoolein was used as a model compound, and its structural changes were probed both *in situ* and *ex situ* which enabled a comparison between different hydration states. A custom-built instrumental configuration allowed the advantages of LFR spectroscopy to be utilized for dynamic hydration analysis. On the other hand, static measurements of equilibrated systems (*i.e.*, with varied aqueous content) showcased the structural sensitivity of LFR spectroscopy. The subtle differences not intuitively observed between similar self-assembled architectures were distinguished by chemometric analysis that directly correlated with the results from small-angle X-ray scattering (SAXS), which is the current "gold standard" method for determining the structure of such materials.
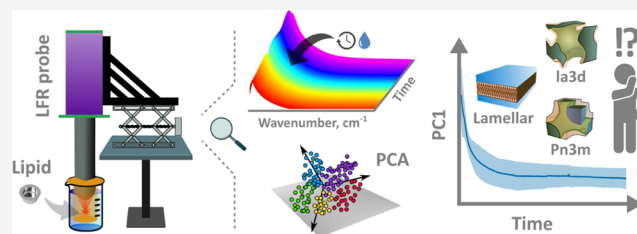
INTRODUCTION

Lipid–water mesophases or lyotropic liquid crystals are a unique state of matter between conventional solids and isotropic liquids, encompassing both structural order and mobility.[1,2] Typically formed when lipid-based amphiphiles are exposed to water, they form a series of self-assembled large-scale architectures that can be tailored for a range of applications, including controlled drug delivery.[1] For example, apart from bilayer-based lamellar phases, they can also form various non-lamellar assemblies consisting of well-defined networks of aqueous channels and lipid bilayer membranes, including the bicontinuous cubic and inverse hexagonal mesophases.[2,3] Various physiologically relevant factors such as temperature, presence of endogenous amphiphilic molecules such as bile salts, water content, and pH, among others, can further induce subtle changes to the self-assembled structure or even global transformations between different structures at equilibrium, both of which are important to understand in detail.[1] However, due to their high complexity, only a limited number of instrumental techniques have been found useful for the characterization of these systems, particularly in a time-resolved manner to study dynamics.

Small-angle X-ray scattering (SAXS), especially synchrotron-based SAXS instrumentation for time-resolved studies, is regarded as the "gold standard" method for determining the structure of self-assembled lipid mesophases as it offers high intrinsic sensitivity to structural information.[4−6] However, the restricted (and costly) access to synchrotron facilities, particularly for industry, limits more rapid advancement in the field and certainly precludes its use in a quality manufacturing context. Additionally, laboratory-based SAXS instruments typically offer limited flexibility for fast temporal

analysis due to the prolonged measurement times required to obtain scattering data of sufficient quality. Consequently, low-frequency Raman (LFR) spectroscopy is proposed to serve as a novel and accessible alternative for understanding the characteristics and behavior of such systems.

LFR spectroscopy (otherwise known as low-wavenumber or THz-Raman spectroscopy; <300 cm^{-1}) can be regarded as a modern extension to the already extensively used mid-frequency Raman (MFR) spectroscopy (300−1800 cm^{-1}) in the field of pharmaceutics.[7] Accordingly, this technique shares all the attractive advantages of MFR spectroscopy such as the non-destructive nature of the measurements, high specificity, and fast measurement time among others. However, the LFR domain probes low-energy intermolecular vibrations that are highly sensitive to structural characteristics, with crystalline systems exhibiting sharp phonon modes (optic phonons), and disordered systems displaying a broad vibrational density of states (VDOS) feature encompassing multiplex information.[7] The recent advances in holographic volume Bragg Gratings necessary to access the LFR region for dispersive Raman systems have allowed further experimental exploitation.[7,8] For example, the LFR region has shown advantages for both polytypic discrimination and quantification, which possess unique crystalline substances that differ only in one of the
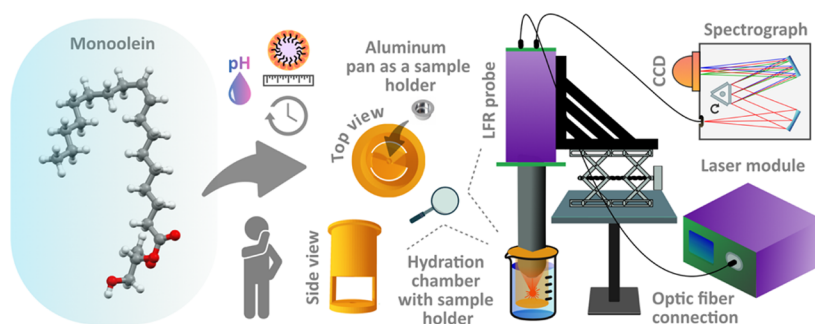
Figure 1. Schematic for the *in situ* LFR instrumental configuration used to collect data during the monitoring of the hydration dynamics of monoolein. A custom-made, 3D-printed chamber was used to house the sample that was placed inside an aluminum pan to avoid significant background Raman signatures for the measurements.

dimensions of the cell unit.[9] Similarly, this technique can be successfully applied for the analysis of amorphous pharmaceutical materials, where even critical information about their global and local molecular mobility governing their physical stability can be obtained.[10] Our previous work has further highlighted the structural sensitivity of this technique by enabling direct monitoring of drug solubilization in complex media such as milk or infant formula, which showed comparable results to synchrotron SAXS.[11,12] However, to the best of our knowledge, LFR spectroscopy has not yet been explored for the dynamic analysis of self-assembled lipid systems. In fact, there is only limited information available in the literature regarding the general application of Raman spectroscopy for such systems, typically restricted to baseline characterization of their equilibrated states.[13,14]

For this proof-of-principle study, monoolein, a well-characterized model system, was selected. As such, its phase transitions upon hydration (among other factors) under a variety of conditions are well understood.[5,15,16] For ambient conditions explored here (~20 °C), monoolein forms a series of structures with increased water content. Upon initial low levels of hydration, a solid crystalline phase (L_C) is formed, followed by a lamellar liquid crystal phase (L_α), then two different bicontinuous cubic V_2-type phases ($Ia3d$ and $Pn3m$) with increasing levels of hydration up to the swelling limit of the V_2 phases at approximately 40% w/w water.[15] Dynamic LFR measurements were primarily used to explore these characteristics and were complimented by the analyses of a series of equilibrated monoolein samples containing different water contents using both Raman spectroscopy and SAXS to establish a potential correlation between the spectral responses in the LFR domain and the unique X-ray scattering profiles (*i.e.*, Bragg peaks) for each of the mesophases.

EXPERIMENTAL SECTION

Materials. Monoolein (2,3-dihydroxypropyl (9Z)-octadec-9-enoate; ≥99%) was purchased from Nu-Chek-Prep, Inc., Elysian, MN, USA, and its purity was verified *via* gas chromatography analysis. Tris(hydroxymethyl)aminomethane maleate salt, sodium chloride, calcium chloride, and sodium hydroxide (1 M) were purchased from Sigma-Aldrich (Søborg, Denmark). For gas chromatography, sodium chloride, dry methanol, sodium stored under petroleum, and hexane (95%) were purchased from Merck (Søborg, Denmark). Milli-Q-grade water purified through a ELGA PURELAB flex 3 from Veolia (Aubervilliers, France) was used throughout this study.

All purchased materials and chemicals were used directly without further purification.

Static Mesophase Hydration. For *ex situ* hydration measurements of equilibrated systems measured both by SAXS and Raman spectroscopy for the determination of lipid bulk phase behavior at ambient temperature (~20 °C), different lipid and tris buffer solution (TBS; prepared using 50 mM tris(hydroxymethyl)aminomethane maleate salt, 150 mM sodium chloride and 5 mM calcium chloride in water adjusted to pH 7.4 with 1 M sodium hydroxide) ratios (10, 20, 30, 40, 50, and 60% TBS w/w) were weighted into 5 mL glass vials, sealed, vortexed, and heated (~70 °C) with an air gun (3-cycles). After 24 h of equilibration at ambient temperature (~20 °C), small amounts of bulk lipids were transferred into 1.5 mm thick borosilicate glass capillaries (Hilgenberg, Kassel, Malsfeld, Germany), flame sealed, and further secured with a glue gun. For capillaries, the bulk phase was then allowed to equilibrate at ambient temperature (~20 °C) for at least 2 days before SAXS measurements. For the Raman spectroscopy measurements, the hydration-equilibrated samples in glass vials were measured through the glass.

Dynamic Mesophase Hydration. For inspection of the *in situ* hydration of monoolein, a 3D-printed chamber mounted inside a glass beaker with an aluminum pan insert (TA Instruments, New Castle, DE, USA) was utilized. The pan was filled with 35 µL of the molten lipid, which was solidified at ambient temperature (~20 °C) for 30 min and placed inside the pan insert. The 3D printed chamber was then placed in a beaker containing 40 mL TBS, followed by a quick adjustment of focus prior to the Raman measurements.

Raman Spectroscopy. A THz-Raman system (Ondax Inc., Monrovia, CA, USA) was used for collecting Raman data with an excitation source from a 300 mW 785 nm laser module (Ondax Inc., Monrovia, CA, USA). For *in situ* and *ex situ* hydration measurements, backscattered light (180° geometry) was collected using a contact/immersion probe tip (MarqMetrix, Seattle, WA, USA) and a free space optics accessory, respectively. The collected light was filtered through a set of volume Bragg gratings (Ondax Inc., Monrovia, CA, USA) and focused into a spectrograph (Ondax Inc., Monrovia, CA, USA) *via* a fiber-optic cable (Figure 1). The light was then dispersed onto a CCD detector (Andor iVac 316, Oxford Instruments, Abingdon, UK). Spectra were collected at ambient temperature (~20 °C) over the spectral window −870 to 3200 cm^{-1} with a 4−6 cm^{-1} resolution. For *in situ* experiments, each spectrum ($n = 3$) was averaged from 30 scans with an integration time of 0.5 s, whereas for the *ex situ* experiments, each spectrum ($n = 5$) was averaged from 120 scans with an
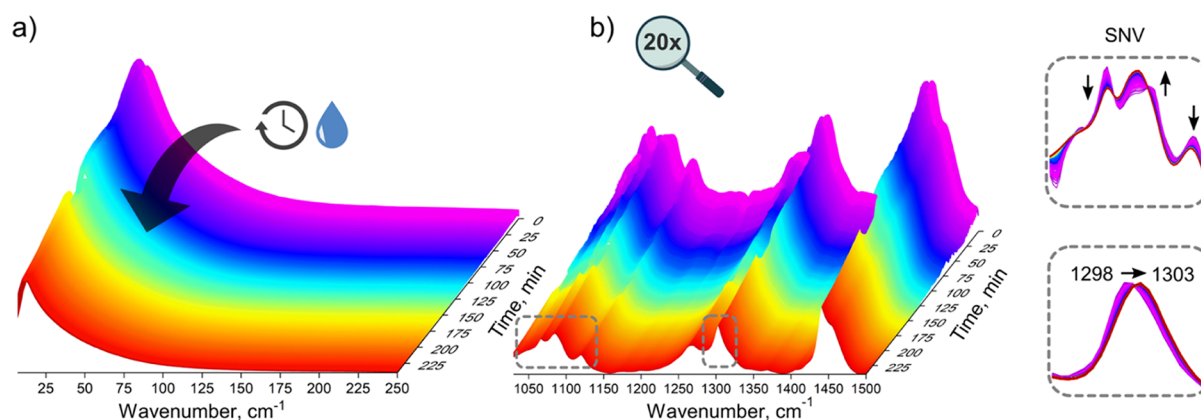
Figure 2. Representative (a) LFR and (b) MFR spectra of monoolein during hydration dynamics at pH 7.4. The individual spectral ranges have been scaled to a maximum intensity for easier comparison (relatively, the LFR domain exhibited at least 20 times higher signal propensity); the insets for the mid-frequency data (SNV corrected for a better visibility of trends) show characteristic changes in the C−C backbone and CH$_2$ twist bands during monoolein hydration.

integration time of 0.5 s. The sample spot size was approximately 0.5−1 mm.

Small-Angle X-Ray Scattering. SAXS measurements were done using a GANESHA instrument from SAXSLAB (Lyngby, Denmark) with a Rigaku (Rigaku-Denki. Co., Tokyo, Japan) 40 W micro-focused Cu source with a wavelength λ of 1.54 Å and a Pilatus 300 k pixel-detector from Dectris (Baden, Switzerland) with a sample-to-detector distance of 441 mm, providing a scattering vector interval of $0.015 < q < 0.65$ Å^{-1}. The samples were in the focus of the X-ray beam for 120 min and exposed to 31 Mph/s. The 2D scattering data were azimuthally averaged into a one-dimensional scattering function using a reduction software (SAXSGUI, Lyngby, Denmark)

$$q = (4\pi/\lambda) \sin (2\theta/2)$$

where q is the scattering vector, λ is the wavelength of the X-ray beam, and 2θ denotes the X-ray scattering angle. The Bragg peaks were described by the lattice parameters (hkl)[17] that were analyzed by an in-house peak fitting algorithm in Python 3.10.0.

Gas Chromatography. This technique was used to investigate the purity of the used monoolein to ensure that impurities were not altering the phase behavior of the lipids. Prior to gas chromatography, monoolein was esterified in a sodium methylate solution and extracted into a hexane phase. The monoolein was loaded into an HP 5890 series II gas chromatograph with FID and an autosampler (7673 GC/SFC Injector) and onto an HP.FFAP column (25 m × 0.20 mm × 0.33 μm); HP, no. 19091F-102 all from Agilent Technologies (Santa Clara, CA, USA). For the analysis, 1 μL of the sample was injected to a 1:8 splitflow with a constant flowrate of 1 mL/min. The injector and detector temperatures were set at 250 and 300 °C, respectively. The oven temperature was first set to 50 °C for 1 min and then increased by 15 °C/min to 180 °C, after which the rate was changed to 5 °C/min to reach the final temperature of 220 °C. This temperature was kept for an additional 10 min.

Data Pre-processing. Raman spectra were first pre-processed using Ondax OSX 1.2.16 software (Ondax Inc., Monrovia, CA, USA) to remove cosmic spikes (≤5 pixel wide). For data collected from samples inside a glass vial, spectra were additionally corrected by subtracting the known

contributions from the glass using the scaled subtraction tool in the same software. Afterward, varied baseline corrections were applied on different spectral domains individually using the spectroscopy module in Orange Data Mining 3.32.0 (University of Ljubljana, Ljubljana, Slovenia) software package.[18] For the low-frequency Raman (LFR) region (−300 to 300 cm^{-1}), a linear baseline correction was applied. However, due to the curved nature of the selected mid-frequency Raman (MFR; 1030 to 1500 cm^{-1}) and C−H stretching (2880−3000 cm^{-1}) regions, a rubberband baseline correction was required. Scale and scattering variations were also amended for each spectral region using the standard normal variate (SNV) transformation in the same software. However, while for the MFR and C−H stretching region data, it was carried out over the same spectral range as the rubberband correction, only a limited window (15−250 or 7−65 cm^{-1}) was used for the LFR domain to process the data obtained from the kinetic studies or equilibrated samples, respectively.

Principal Component Analysis. This chemometric analysis was carried out on the fully pre-processed spectroscopic data in Orange Data Mining 3.32.0 (University of Ljubljana, Ljubljana, Slovenia) software environments using default settings.

Computational Details. Theoretical Raman spectra of monoolein (with or without the external solvent field imitating anhydrous or hydrated environments) were calculated *via* density functional theory (DFT) methodology. For this purpose, the Becke three-parameter exchange and Lee−Yang−Parr correlation B3LYP functional[19,20] with the 6-311+G basis set augmented with a polarization function (d) were employed. The initial molecular representation of monoolein was constructed using Avogadro 1.2 software, and the ground-state geometry optimization in the gas phase with full relaxation on the potential energy surface was carried out at the same level of theory. The resultant geometry was used as an input for further calculations, where the Raman spectrum was calculated in the gas phase as well as with the applied solvent field using the integral equation formalism polarized continuum model (IEFPCM).[21] All computational calculations were executed using the Gaussian 09 software package (revision C.01; Gaussian Inc., CT, USA),[22] the quadratically convergent SCF method, and an ultrafine integration grid without any special adjustments of atomic radii. The
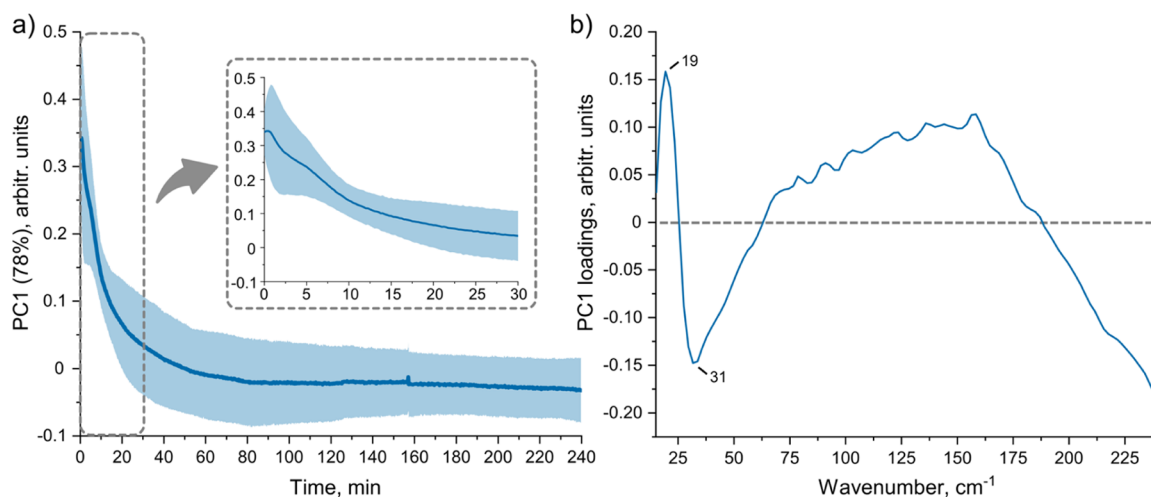
Figure 3. (a) PC1 mean scores of LFR data with standard deviation between replicate runs (shaded; $n = 3$) and (b) the respective loadings plot highlighting changes in the broad VDOS feature upon monoolein hydration.

visualization of the calculated results was performed using the GaussView 5.0 software (Gaussian Inc., CT, USA) and GaussSum.[23] Vibrational spectra from Raman frequency calculations were scaled by 0.975 for the B3LYP functional as previously described[24] and corrected for the utilized laser wavelength (785 nm).

RESULTS AND DISCUSSION

Exploratory Analysis of Hydration Dynamics. In order to investigate the dynamics of monoolein hydration, a modular LFR setup with a probe accessory was used, where the bulk lipid sample was housed inside a custom, 3D-printed chamber (Figure 1). Our 785 nm Raman system allowed us to record spectra over a broad spectral window (-870 to 3200 cm^{-1}), and spectra for dynamic analysis were collected every 15 s (30 accumulations of 0.5 s exposure time) for a total of 4 h. However, it is important to note that with the increased LFR scattering propensity, it was also feasible to record sufficient quality data at our hardware (read/write) limit of 32 ms.

A comparison between LFR and MFR spectral domains for a typical dataset obtained during hydration dynamics is illustrated in Figure 2. Additional data regarding the C−H stretching region is presented in Figure S1. By a qualitative inspection, it was difficult to deduce any substantial changes in the broad VDOS feature <150 cm^{-1}, in part because it also encompassed the spectral signature of the tris buffer solution (TBS) that was used to hydrate the lipid sample. The ionic strength and pH were controlled for the hydration liquid to ensure that dynamics are probed in physiologically relevant conditions. In contrast, the MFR showed some apparent differences in the 1000−1150 and 1280−1320 cm^{-1} spectral range related to the C−C backbone and CH$_2$ twist vibrations, respectively. These bands have been previously identified to be sensitive to structural changes of self-assembled lipid systems containing monoolein.[13,25] Similarly, significant changes in the C−H stretching region could be observed with a gradual decrease and simultaneous growth of peaks at ~2888 and 2895 cm^{-1}, respectively. To better elaborate on these spectral alterations (both here and at the MFR domain), theoretical calculations employing DFT methodology were also carried out. Figure S2 highlights the main results of this analysis using experimental spectra collected at the beginning and end of the

in situ hydration experiments for comparison. It is important to note that despite using a set of computational parameters that typically ensure tight convergence criteria, these theoretical calculations inherited a couple of small imaginary frequencies that are not uncommon for compounds with high degrees of freedom. In this instance, the long alkyl chains of monoolein (Figure 1) make it difficult to find the true minima of the expectedly flat potential energy surface. Nevertheless, the quality of the simulations was at least sufficient to compare general trends, where the biggest alterations were observed at similar spectral domains to the experimental data. Most notably, the DFT calculations showed that in the presence of a solvent field (*i.e.*, water), the largest changes in the C−H stretching region are expected to occur for the alkene fragment, potentially indicating slight shifts in the chain splay upon hydration.

Principal component analysis (PCA) was further utilized to uncover differences between spectra, especially for the LFR domain. This chemometric technique permits a reduction in the number of variables without the concomitant loss of information, with the results represented by scores and loadings. As each spectrum is simplified to a single point in a two-dimensional principal component (PC) space, temporal data points with similar PC scores have related spectral features. Accordingly, loading plots highlight the basis upon which the separation in the PC space has been achieved. Figure 3 highlights the results of this analysis for the LFR spectral range, where PC1 accounted for 78% of the spectral variance and largely resolved changes in the line shape toward the maximum of the VDOS feature (Figure 3b). Overall, there was an exponential change in PC1 scores with time increment that stabilized within 100−120 min (consistent among replicate measurements), representing a pseudo-equilibrated state of monoolein. These results were complimented by a similar analysis of MFR (Figure S3) and C−H stretching region (Figure S4) data, where the aforementioned spectral changes (*i.e.*, visually observed peak shifts) were highlighted by the PC1, exemplifying almost identical temporal characteristics.

It is interesting to note that in all cases (more pronounced in the LFR data likely due to its higher structural sensitivity and overall signal propensity), a small but consistent "ladder-shaped" change was observed within the first 5−10 min that might indicate the formation of intermediate states. As noted
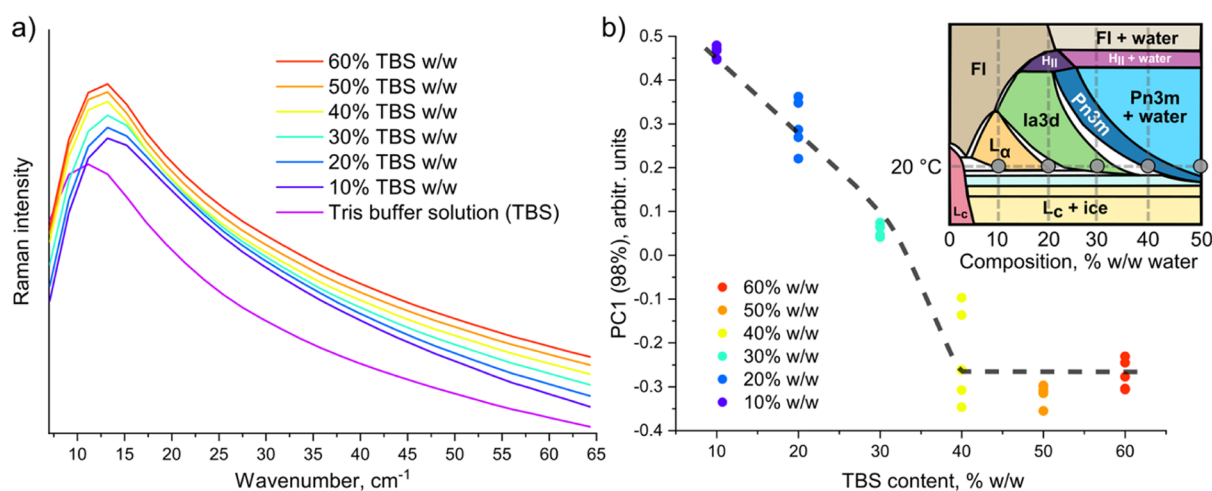
Figure 4. Examples of (a) LFR spectra (SNV corrected and offset for better visibility of trends) of the tris buffer solution (TBS) and the monoolein equilibrated at ambient conditions (~20 °C) with different quantities of TBS and (b) PC1 scores of LFR data ($n = 5$) illustrating different changes with increasing TBS content; the line is drawn to assist in visualizing the trend. The inset diagram shows an equilibrium temperature-composition phase diagram for the monoolein/water system that was redrawn from data by Qiu and Caffrey[15] with permission from Elsevier using a similar illustration style as presented elsewhere.[26]

previously, monoolein undergoes several phase transformations with an incremental increase in water content.[15] To understand and explore this phenomenon in greater detail, a series of equilibrated monoolein samples with different aqueous tris buffer contents were analyzed using LFR spectroscopy and SAXS to establish a potential correlation between the techniques, and, hence, potentially observed states during the dynamic hydration analysis.

Figure 4a shows a series of representative LFR spectra for these samples that, even visually, exhibited noticeable differences, specifically the broad change in the peak shape and the redshift with increasing buffer content. This was better exemplified by the PCA, where PC1 score values trended toward negative PC space with increasing buffer content within the sample (Figure 4b) and coincided with the aforementioned VDOS feature changes based on the PC1 loadings plot (Figure S5). Although the aqueous buffer solution also has a characteristic VDOS feature in the LFR domain (Figure 4), its mere increase could not cause the observed nonlinear spectral response. Instead, given the complex nature of the monoolein phase diagram (Figure 4b inset), LFR was assumed to probe different self-assembled architectures that also coincided with the fact that no further changes in the mesophase structure are expected to occur beyond 40% w/w aqueous content at ~20 °C. Interestingly, unlike with dynamic analysis, no correlation to the MFR domain or the C−H stretching region could be established, as practically identical spectral responses were obtained in the traditionally used instrumental configurations (Figures S6a and S7a). This observation was confirmed by the PCA, which showed a random distribution among the samples (Figures S6 and S7) with loadings plots for the main components (PC1, PC2, and PC3), largely explaining the variance associated with the signal noise (Figures S8 and S9). The broad peak (~1275−1500 cm^{-1}) resolved in the positive PC1 space for the MFR data could be related to the remaining small contributions from the glass vial (Figure S10) that were subtracted during the data preprocessing. However, while no differences between equilibrated samples in the MFR or C−H stretching spectral ranges were established, the spectral profiles themselves (even

at 10% w/w) were identical to the ones recorded at the end of the dynamic hydration experiments (Figures 2b and S1). This observation has two major implications: (i) only a limited amount of hydration had been achieved during the monitored hydration dynamics compared to the static samples that were analyzed after extended equilibration time; (ii) it is likely that conventional frequency domains are only capable of detecting hydration per se and not the detailed transition states. Considering that typical Raman spectroscopy (>300 cm^{-1}) probes intramolecular motions (*i.e.*, local environment), this finding is, in retrospect, not unexpected.

Structural Analysis Using SAXS for Correlation with LFR Spectroscopy. The complementary SAXS results (Figure 5) showed that a lamellar liquid crystal phase had formed at 10 and 20% w/w aqueous content, indicated by the evenly spaced diffraction peaks at $q \sim 0.17$ and 0.34 Å^{-1} corresponding with the general expectations from the phase diagram. However, there was a slight downshift in q-values resulting in a ~1 Å greater distance between the layers for a more hydrated sample (*i.e.*, 20% w/w). These subtle differences were also distinguished by the LFR spectroscopy, highlighting its comparable sensitivity to SAXS. This may indicate that LFR spectroscopy could even be suitable for the analysis of dispersed liquid crystalline phases, where composition-induced lattice parameter changes are currently of particular interest[27] and could serve as an accessible avenue for subsequent studies where a SAXS experiment may not be possible. The 30% w/w sample contained a V$_2$(Ia3d) phase, with the primary peaks indicating the cubic phase at spacing ratios of $\sqrt{6}$, $\sqrt{8}$, $\sqrt{14}$, and $\sqrt{16}$, whereas at hydration levels of 40, 50, and 60% w/w, the SAXS diffractograms displayed features characteristic of the V$_2$ cubic phase with the *Pn3m* spacegroup and peaks at spacing ratios of $\sqrt{2}$, $\sqrt{3}$, $\sqrt{4}$, $\sqrt{6}$, $\sqrt{8}$, and $\sqrt{9}$. All of these results were coincident with features in the LFR data in Figure 4b, particularly for higher states of hydration where samples possessing the same structures (>40% w/w) exhibited almost identical PC score values and, hence, indicated similar structural properties.

To further investigate the correlation between the LFR data (*i.e.*, PC1 score values) and the content of the aqueous phase
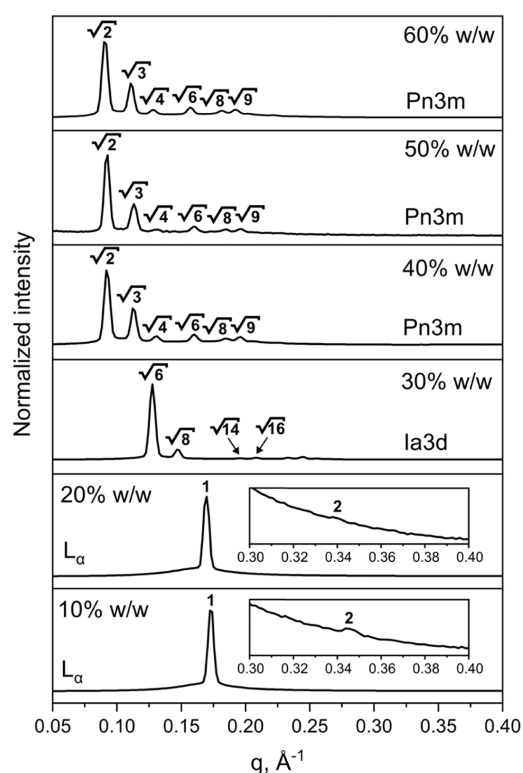
Figure 5. SAXS patterns of the monoolein samples equilibrated at ambient conditions (~20 °C) with different quantities of TBS (%, w/w).

in both the lamellar (Lα) and cubic (Ia3d and Pn3m space groups) phases, the water layer distances between the bilayers were calculated. The methodology of these calculations is described in detail in the Supporting Information. A clear correlation was observed to the bilayer distance extrapolated from SAXS measurements, yielding an R^2 value of 0.97 (Figure S11), which points to the capability of LFR spectroscopy to give physical insights into the swelling behavior of lipid mesophases. Accordingly, it could already be used as a screening tool to quickly identify structural differences, or at least attainment of equilibrium, that can further be probed with SAXS. For lipid-based pharmaceutical formulation development, it may enable a new accessible approach to formulation screening for compositions with desired structural or hydration attributes for drug delivery applications.

Significance. Based on these results, the limited interference from the aqueous medium, high structural sensitivity, and fast measurement time suggests LFR spectroscopy to be an attractive avenue for investigating self-assembled molecular architectures. Besides the technical capabilities, LFR spectroscopy also offers practical benefits with less demanding sample-handling requirements when compared to, for example, SAXS. With this technique, a water gradient is usually achieved by placing the sample at the bottom of a glass capillary and covering it with an aqueous phase, where discrete points are then analyzed along the capillary axis.[28] These experiments can not only be challenging if more viscous samples are being analyzed but also require complementary techniques such as cross-polarized light microscopy to be used in order to verify the presence of phases that occur at a narrow concentration range that may be completely missed by the scanning X-ray beam.[28] The ability of LFR spectroscopy to easily collect data

from different instrumental arrangements (*i.e.*, optical geometries) and different sample holders, including opaque ones by utilizing macro- or micro-scale spatially offset setups,[29,30] offers higher experimental flexibility. In fact, with commercial options for incorporating LFR capabilities into Raman microscopes, multimodal imaging could be used for comparable analysis. Similar flexibility of spectroscopic techniques has also been highlighted by Laughlin *et al.*, who presented the capabilities of near-infrared (NIR) spectroscopy to detect subtle changes in water content with increasing aqueous phase content.[31] Recently, Yao *et al.* used broadband dielectric spectroscopy (BDS) to investigate different water states of monolinolein (a close analogue of monoolein)—further broadening the portfolio of spectroscopic techniques useful for the characterization of mesophases.[32] However, considering the general complexity of the observed spectral responses from LFR spectroscopy that, in this instance, required a use of simple chemometric analysis to extract useful information, a knowledge base for the interpretation of the LFR data needs to be established by exploring an array of systems, where machine learning approaches could also be utilized for dissecting the perturbations of mesophase constructs.[33] This also includes thermotropic liquid crystals, where the response in the spectral variety should be even more pronounced, presenting an opportunity to probe finite changes in very short timescales. This aspect, given the aforementioned advantages, should enable LFR spectroscopy to emerge as research and an in-line analytical tool within pharmaceutical manufacturing for quality control purposes.

■ CONCLUSIONS

The potential of LFR spectroscopy was assessed for the discrimination of different structures formed upon the self-assembly of lipid systems due to hydration. Monoolein was used as a model compound due to its well-understood behavior, and the LFR results were complimented by SAXS analysis that revealed a direct correlation between both techniques when static samples with known quantities of the aqueous phase were compared. These findings allude to at least a potential application of LFR spectroscopy as a screening tool within the pharmaceutical sector, where such self-assembled systems are used for drug delivery purposes. However, a knowledge base in LFR spectral data interpretation needs to be established with subsequent studies to grasp the full capabilities of this technique for more comprehensive analysis.

■ ASSOCIATED CONTENT

Ⓢ Supporting Information

The Supporting Information is available free of charge at https://pubs.acs.org/doi/10.1021/acs.jpcb.2c08150.

> Description of calculations for lipid length and water channel characteristics, data representation of the C−H stretching region during hydration dynamics, DFT simulations of monoolein emulating non-hydrated/hydrated conditions, information about the PCA of MFR and C−H stretching region data of monoolein hydration dynamics, PCA loadings plot of LFR data (PC1) of equilibrated monoolein−aqueous tris buffer solution mixtures, MFR and C−H stretching region spectrum examples and PCA loadings plots (PC1, PC2, and PC3) of respective data of equilibrated monoolein−aqueous tris buffer solution mixtures, Raman spectrum

example of a glass vial used for equilibrated monoolein–aqueous tris buffer solution mixtures, and comparison and correlation analysis between LFR and SAXS data (PDF)

■ AUTHOR INFORMATION

Corresponding Authors

Ben J. Boyd − *Department of Pharmacy, Faculty of Health and Medical Sciences, University of Copenhagen, Copenhagen 2100, Denmark; Drug Delivery, Disposition and Dynamics, Monash Institute of Pharmaceutical Sciences, Parkville, Victoria 3052, Australia;* ⊙ orcid.org/0000-0001-5434-590X; Email: ben.boyd@sund.ku.dk

Kārlis Bērziņš − *Department of Pharmacy, Faculty of Health and Medical Sciences, University of Copenhagen, Copenhagen 2100, Denmark;* ⊙ orcid.org/0000-0001-6545-5522; Email: karlis.berzins@sund.ku.dk

Authors

Lasse S. Krog − *Department of Pharmacy, Faculty of Health and Medical Sciences, University of Copenhagen, Copenhagen 2100, Denmark;* ⊙ orcid.org/0000-0001-9444-1517

Jacob J. K. Kirkensgaard − *Department of Food Science, Faculty of Science, University of Copenhagen, Frederiksberg C 1958, Denmark; Niels Bohr Institute, Faculty of Science, University of Copenhagen, Copenhagen 2100, Denmark;* ⊙ orcid.org/0000-0001-6265-0314

Vito Foderà − *Department of Pharmacy, Faculty of Health and Medical Sciences, University of Copenhagen, Copenhagen 2100, Denmark;* ⊙ orcid.org/0000-0003-2855-0568

Complete contact information is available at:
https://pubs.acs.org/10.1021/acs.jpcb.2c08150

Notes

The authors declare no competing financial interest.

■ ACKNOWLEDGMENTS

■ REFERENCES

(1) Mo, J.; Milleret, G.; Nagaraj, M. Liquid crystal nanoparticles for commercial drug delivery. *Liq. Cryst. Rev.* **2017**, *5*, 69−85.

(2) Chountoulesi, M.; Pispas, S.; Tseti, I. K.; Demetzos, C. Lyotropic Liquid Crystalline Nanostructures as Drug Delivery Systems and Vaccine Platforms. *Pharmaceuticals* **2022**, *15*, 429.

(3) Kaasgaard, T.; Drummond, C. J. Ordered 2-D and 3-D nanostructured amphiphile self-assembly materials stable in excess solvent. *Phys. Chem. Chem. Phys.* **2006**, *8*, 4957−4975.

(4) Vita, F.; Adamo, F. C.; Pisani, M.; Francescangeli, O. Nanostructure of Unconventional Liquid Crystals Investigated by Synchrotron Radiation. *Nanomaterials* **2020**, *10*, 1679.

(5) Conn, C. E.; Ces, O.; Squires, A. M.; Mulet, X.; Winter, R.; Finet, S. M.; Templer, R. H.; Seddon, J. M. A Pressure-Jump Time-Resolved X-ray Diffraction Study of Cubic—Cubic Transition Kinetics in Monoolein. *Langmuir* **2008**, *24*, 2331−2340.

(6) Salentinig, S.; Zabara, M.; Parisse, P.; Amenitsch, H. Formation of highly ordered liquid crystalline coatings—an in situ GISAXS study. *Phys. Chem. Chem. Phys.* **2018**, *20*, 21903−21909.

(7) Bērziņš, K.; Fraser-Miller, S. J.; Gordon, K. C. Recent Advances in Low-Frequency Raman Spectroscopy for Pharmaceutical Applications. *Int. J. Pharm.* **2021**, *592*, 120034.

(8) Glebov, A. L.; Mokhun, O.; Rapaport, A.; Vergnole, S.; Smirnov, V.; Glebov, L. B. Volume Bragg Gratings as Ultra-narrow and Multiband Optical Filters. *SPIE Photonics Europe 2012*; Brussels, Belgium, 2012; Vol. *8428*.

(9) Iwata, K.; Karashima, M.; Ikeda, Y.; Inoue, M.; Fukami, T. Discrimination and quantification of sulfathiazole polytypes using low-frequency Raman spectroscopy. *CrystEngComm* **2018**, *20*, 1928−1934.

(10) Bērziņš, K.; Fraser-Miller, S. J.; Rades, T.; Gordon, K. C. Low-Frequency Raman Spectroscopy as an Avenue to Determine the Transition Temperature of β- and γ-Relaxation in Pharmaceutical Glasses. *Anal. Chem.* **2022**, *94*, 8241−8248.

(11) Salim, M.; Fraser-Miller, S. J.; Sutton, J. J.; Bērziņš, K.; Hawley, A.; Clulow, A. J.; Beilles, S.; Gordon, K. C.; Boyd, B. J. Application of Low-Frequency Raman Scattering Spectroscopy to Probe in Situ Drug Solubilization in Milk during Digestion. *J. Phys. Chem. Lett.* **2019**, *10*, 2258−2263.

(12) Salim, M.; Fraser-Miller, S. J.; Bērziņš, K.; Sutton, J. J.; Ramirez, G.; Clulow, A. J.; Hawley, A.; Beilles, S.; Gordon, K. C.; Boyd, B. J. Low-Frequency Raman Scattering Spectroscopy as an Accessible Approach to Understand Drug Solubilization in Milk-Based Formulations during Digestion. *Mol. Pharm.* **2020**, *17*, 885−899.

(13) Suga, K.; Otsuka, Y.; Okamoto, Y.; Umakoshi, H. Gel-Phase-like Ordered Membrane Properties Observed in Dispersed Oleic Acid/1-Oleoylglycerol Self-Assemblies: Systematic Characterization Using Raman Spectroscopy and a Laurdan Fluorescent Probe. *Langmuir* **2018**, *34*, 2081−2088.

(14) Valldeperas, M.; Talaikis, M.; Dhayal, S. K.; Velička, M.; Barauskas, J.; Niaura, G.; Nylander, T. Encapsulation of Aspartic Protease in Nonlamellar Lipid Liquid Crystalline Phases. *Biophys. J.* **2019**, *117*, 829−843.

(15) Qiu, H.; Caffrey, M. The phase diagram of the monoolein/water system: metastability and equilibrium aspects. *Biomaterials* **2000**, *21*, 223−234.

(16) Rittman, M.; Amenitsch, H.; Rappolt, M.; Sartori, B.; O'Driscoll, B. M. D.; Squires, A. M. Control and Analysis of Oriented Thin Films of Lipid Inverse Bicontinuous Cubic Phases Using Grazing Incidence Small-Angle X-ray Scattering. *Langmuir* **2013**, *29*, 9874−9880.

(17) Hyde, S. T. Identification of lyotropic liquid crystalline mesophases. *Handbook of applied surface and colloid chemistry*; Wiley, 2001; Vol. *2*, pp 299−332.

(18) Demšar, J.; Curk, T.; Erjavec, A.; Gorup, C.; Hocevar, T.; Milutinovic, M.; Mozina, M.; Polajnar, M.; Toplak, M.; Staric, A.; et al. Orange Data: Mining Toolbox in Python. *J. Mach. Learn. Res.* **2013**, *14*, 2349−2353.

(19) Becke, A. D. Density-functional thermochemistry. III. The role of exact exchange. *J. Chem. Phys.* **1993**, *98*, 5648−5652.

(20) Lee, C.; Yang, W.; Parr, R. G. Development of the Colle-Salvetti correlation-energy formula into a functional of the electron density. *Phys. Rev. B* **1988**, *37*, 785−789.

(21) Scalmani, G.; Frisch, M. J. Continuous surface charge polarizable continuum models of solvation. I. General formalism. *J. Chem. Phys.* **2010**, *132*, 114110.

(22) Frisch, M.; Trucks, G.; Schlegel, H.; Scuseria, G.; Robb, M.; Cheeseman, J.; Scalmani, G.; Barone, V.; Mennucci, B.; Petersson, G.; et al. *Gaussian 09*; Revision C01; Gaussian Inc., 2010.

(23) O'boyle, N. M.; Tenderholt, A. L.; Langner, K. M. A library for package-independent computational chemistry algorithms. *J. Comput. Chem.* **2008**, *29*, 839−845.

(24) Scott, A. P.; Radom, L. Harmonic Vibrational Frequencies: An Evaluation of Hartree—Fock, Møller—Plesset, Quadratic Configuration Interaction, Density Functional Theory, and Semiempirical Scale Factors. *J. Phys. Chem.* **1996**, *100*, 16502−16513.

(25) Razumas, V.; Talaikytė, Z.; Barauskasa, J.; Larsson, K.; Miezis, Y.; Nylander, T. Effects of distearoylphosphatidylglycerol and lysozyme on the structure of the monoolein-water cubic phase: X-ray diffraction and Raman scattering studies. *Chem. Phys. Lipids* **1996**, *84*, 123−138.

(26) Ishchenko, A.; Abola, E.; Cherezov, V. Lipidic Cubic Phase Technologies for Structural Studies of Membrane Proteins. In *Membrane Proteins Production for Structural Analysis*; Mus-Veteau, I., Ed.; Springer: New York, 2014; pp 289−314.

(27) Huang, Y.; Gui, S. Factors affecting the structure of lyotropic liquid crystals and the correlation between structure and drug diffusion. *RSC Adv.* **2018**, *8*, 6978−6987.

(28) Liu, C. K.; Warr, G. G. Hexagonal closest-packed spheres liquid crystalline phases stabilised by strongly hydrated counterions. *Soft Matter* **2014**, *10*, 83−87.

(29) Bērziņš, K.; Fraser-Miller, S. J.; Gordon, K. C. A New Frontier for Nondestructive Spatial Analysis of Pharmaceutical Solid Dosage Forms: Spatially Offset Low-Frequency Raman Spectroscopy. *Anal. Chem.* **2021**, *93*, 3698−3705.

(30) Bērziņš, K.; Fraser-Miller, S. J.; Gordon, K. C. Pseudo-3D Subsurface Imaging of Pharmaceutical Solid Dosage Forms Using Micro-spatially Offset Low-Frequency Raman Spectroscopy. *Anal. Chem.* **2021**, *93*, 8986−8993.

(31) Laughlin, R. G.; Lynch, M. L.; Marcott, C.; Munyon, R. L.; Marrer, A. M.; Kochvar, K. A. Phase Studies by Diffusive Interfacial Transport Using Near-Infrared Analysis for Water (DIT-NIR). *J. Phys. Chem. B* **2000**, *104*, 7354−7362.

(32) Yao, Y.; Catalini, S.; Kutus, B.; Hunger, J.; Foggi, P.; Mezzenga, R. Probing Water State during Lipidic Mesophases Phase Transitions. *Angew. Chem., Int. Ed.* **2021**, *60*, 25274−25280.

(33) Meza Ramirez, C. A.; Greenop, M.; Ashton, L.; ur Rehmana, I. Applications of machine learning in spectroscopy. *Appl. Spectrosc. Rev.* **2021**, *56*, 733−763.

📖 Recommended by ACS